tional frequencies. The studies of Cooper *et al.* have also shown that the leading many-body dispersion and induction terms are *not* expected to be large enough to resolve these discrepancies. However, exchange repulsion between the two argon atoms results in the generation of multipole moments, which can in turn interact with the permanent moments of the HCl constituent. This particular three-body term is indeed large enough to account for the observed deviations from pairwise additivity. Future efforts are likely to yield a precise description of these exchange-induced multipole forces.

Concluding Remarks

The study of intermolecular forces has entered a new era. It is now possible to place nearly any conceivable functional group into the gas phase with supersonic jet technology. Furthermore, with the development of tunable FIR lasers, a general spectroscopic technique which probes the degrees of freedom that are most intimately related to the intermolecular potential energy surface has become available.

Theoretically, it is now possible, in principle, to directly invert high-resolution cluster spectra, although for systems of low symmetry the computational requirements are prodigious. The development of improved methods for eigenvalue generation on complicated, multidimensional potential energy surfaces can therefore be expected to have an enormous impact on not only intermolecular interactions but intramolecular dynamics as well. Nevertheless, the means to generate experimentally accurate, fully anisotropic representations of intermolecular forces, including the critical role of nonpairwise contributions, are now clearly at hand. The newly developed view of van der Waals and hydrogen bond VRT dynamics has revealed the delicate interplay between the attractive and repulsive terms in intermolecular potentials. By elucidating the true character of weak interactions, these powerful tools will enable scientists to examine the molecular details of a multitude of chemical and biological processes at unprecedented levels of accuracy and detail.

REFERENCES AND NOTES

1. D. D. Nelson, G. T. Fraser, W. Klemperer, *Science* **238**, 1670 (1987).
2. R. J. Saykally, *Acc. Chem. Res.* **22**, 295 (1989); R. C. Cohen and R. J. Saykally, *J. Phys. Chem.* **96**, 1024 (1992).
3. G. A. Blake *et al.*, *Rev. Sci. Instrum.* **62**, 1693 (1991); *ibid.*, p. 1701.
4. P. Verhoeve *et al.*, *ibid.* **61**, 1612 (1990).
5. D. W. Firth, M. A. Dvorak, S. W. Reeve, R. S. Ford, K. R. Leopold, *Chem. Phys. Lett.* **168**, 161 (1990).
6. R. E. Miller, *Science* **240**, 447 (1988); D. J. Nesbitt, in *Dynamics of Polyatomic van der Waals Complexes*, N. Halberstadt and K. C. Janda, Eds. (Plenum, New York, 1990), pp. 461–470.
7. S. Novick, K. Leopold, W. Klemperer, in *Atomic and Molecular Clusters*, E. R. Bernstein, Ed. (Elsevier, New York, 1990), pp. 359–391.
8. R. C. Cohen and R. J. Saykally, *Annu. Rev. Phys. Chem.* **42**, 369 (1991).
9. J. M. Hutson, *ibid.* **41**, 123 (1990).
10. ———, *J. Phys. Chem.* **96**, 4237 (1992).
11. M. J. Elrod, B. C. Host, D. W. Steyert, R. J. Saykally, *Mol. Phys.*, in press.
12. R. C. Cohen and R. J. Saykally, *J. Chem. Phys.*, in press.
13. C. A. Schmuttenmaer *et al.*, in preparation.
14. H. O. Leung, M. D. Marshall, R. D. Suenram, F. J. Lovas, *J. Chem. Phys.* **90**, 700 (1989); D. Yaron *et al.*, *ibid.* **92**, 7095 (1990).
15. R. E. Bumgarner, S. Suzuki, P. A. Stockman, P. G. Green, G. A. Blake, *Chem. Phys. Lett.* **176**, 123 (1991).
16. R. E. Bumgarner, J. Bowen, G. A. Blake, in preparation.
17. P. A. Stockman, R. E. Bumgarner, S. Suzuki, G. A. Blake, *J. Chem. Phys.* **96**, 2496 (1992).
18. L. Dore *et al.*, in preparation.
19. D. Steyert *et al.*, in preparation.
20. M. F. Perutz, in *The Chemical Bond*, A. Zewail, Ed. (Academic Press, New York, 1992), pp. 17–30.
21. S. Suzuki *et al.*, *Science* **257**, 942 (1992).
22. D. Rodham *et al.*, *Nature*, in press.
23. G. C. Pimentel and A. L. McClellan, *The Hydrogen Bond* (Freeman, San Francisco, 1960), pp. 202–203.
24. T. R. Dyke, B. J. Howard, W. Klemperer, *J. Phys. Chem.* **56**, 2442 (1972).
25. S. C. Althorpe, D. C. Clary, P. R. Bunker, *Chem. Phys. Lett.* **187**, 345 (1991).
26. J. A. Odutola, T. A. Hu, D. A. Prinslow, S. E. O'dell, T. R. Dyke, *J. Chem. Phys.* **88**, 5352 (1988).
27. G. T. Fraser, *Int. Rev. Phys. Chem.* **10**, 189 (1991); and references therein.
28. N. Pugliano and R. J. Saykally, *J. Chem. Phys.* **96**, 1832 (1992); N. Pugliano, J. D. Cruzan, J. G. Loeser, R. J. Saykally, *ibid.*, in press.
29. N. Pugliano and R. J. Saykally, *Science* **257**, 1937 (1992).
30. J. G. Loeser *et al.*, *J. Chem. Phys.* **97**, 4727 (1992).
31. J. W. I. van Bladel, A. van der Avoird, P. E. S. Wormer, R. J. Saykally, *ibid.*, p. 4750.
32. D. D. Nelson and W. Klemperer, *ibid.* **87**, 139 (1987); and references therein.
33. G. A. Blake and R. E. Bumgarner, *ibid.* **91**, 7300 (1989).
34. G. C. Maitland, M. Rigby, E. B. Smith, W. A. Wakeham, *Intermolecular Forces: Their Origin and Determination* (Oxford Univ. Press, Oxford, 1987).
35. M. J. Elrod, D. W. Steyert, R. J. Saykally, *J. Chem. Phys.* **94**, 58 (1991); *ibid.* **95**, 3182 (1991); M. J. Elrod, J. G. Loeser, R. J. Saykally, *ibid.*, in press.
36. A. R. Cooper and J. M. Hutson, *ibid.*, in press.
37. R. E. Bumgarner and G. A. Blake, *Chem. Phys. Lett.* **161**, 308 (1989).

38. We thank the many graduate students and postdoctoral fellows at Berkeley and Caltech whose efforts made this research possible. The FIR-VRTS program at Berkeley is supported by NSF grant CHE-9123335, and at Caltech by NSF grant CHE-8957228. G.A.B. also acknowledges support from the David and Lucille Packard and Alfred P. Sloan Foundations.

Electronic Structure Contributions to Function in Bioinorganic Chemistry

Edward I. Solomon* and Michael D. Lowery

Many metalloenzymes exhibit distinctive spectral features that are now becoming well understood. These reflect active site electronic structures that can make significant contributions to catalysis. Copper proteins provide well-characterized examples in which the unusual electronic structures of their active sites contribute to rapid, long-range electron transfer reactivity, oxygen binding and activation, and the multielectron reduction of dioxygen to water.

Many enzymes and proteins have metal ions at their active sites that play key roles in catalysis. Metal ions can mediate facile electron transfer reactions and are capable of binding and activating small molecules, such as O_2 and N_2. The active sites of many metalloproteins exhibit distinctive spectral features as compared with small molecule inorganic complexes of the same metal ion. These features are a result of the unusual geometric and electronic structures that can be imposed on a metal ion in a protein environment. One of the major goals of research in bioinorganic chemistry has been to understand the origin of these spectral features and to use this information to generate a working model of the geometric structure of the active site in the absence of x-ray crystallographic information.

In the last decade, the crystal structures of many metalloproteins have become available at atomic resolutions. One notable example is the recently reported structure of the Fe-Mo cofactor of nitrogenase (*1*). Accurate determination of the geometric structure is, of course, a critically important goal; however, far from being the culmination of research in the bioinorganic chemistry of a class of metalloproteins, it is the starting point for fundamental studies directed toward understanding biological function at a molecular level. The focus of our research has been to combine the results of a variety of spectroscopic methods with a quantum

The authors are in the Department of Chemistry, Stanford University, Stanford, CA 94305.

*To whom correspondence should be addressed.

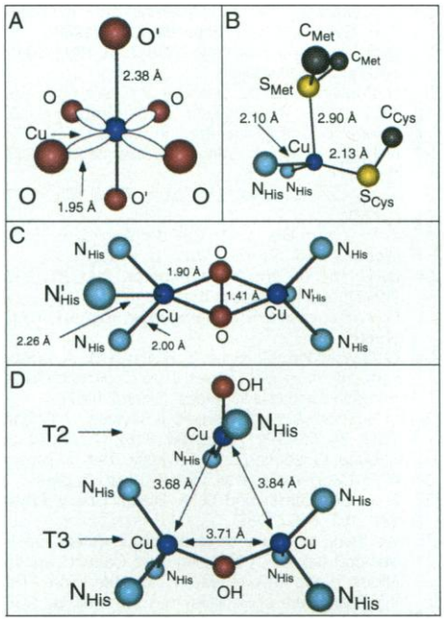

Fig. 1. Copper geometries. (**A**) The normal Cu site of the tetragonal $Cu(H_2O)_6^{2+}$ cation. The equatorial ligands are designated O and the axial O′ (the H atoms have been omitted for clarity). The highest energy, half-occupied Cu $d_{x^2-y^2}$ orbital is superimposed on the molecular frame. (**B**) The blue Cu site in poplar plastocyanin (*11*). (**C**) The coupled binuclear site in oxygenated arthropod hemocyanin (*12*); details of the bound peroxide are based on the structure of the $\mu - \eta^2:\eta^2$ Cu complex prepared by Kitajima *et al.* (*15*). The axial N'_{His} atoms are above and below the Cu-O_2-Cu plane. (**D**) The trinuclear Cu cluster in the multicopper oxidase, ascorbate oxidase (*10*). The T1 Cu site (not pictured) is ~12.5 Å from the T3 Cu atoms, opposite the T2 center.

mechanical description of bonding and to correlate this with a reasonably precise geometric structure to obtain detailed insight into the electronic structure of an active site (*2*, *3*). The distinctive spectral features associated with many classes of metalloprotein active sites reflect electronic structures that can make major contributions to the biological reactivity of these sites.

When discussing the spectral features of metalloproteins, numerous types of spectroscopy, spanning many orders of magnitude in energy, can be considered. Transition-metal complexes usually have partially filled *d* orbitals that often result in paramagnetic ground states that can be studied with electron paramagnetic resonance (EPR) spectroscopy and magnetic susceptibility, even when the metal ion is incorporated in a large, diamagnetic protein environment. Transition metal complexes also exhibit low-energy ligand field transitions in which electrons are excited between the partially filled *d* orbitals. These transitions contribute to the visible absorption spectrum with moderate intensities (molar extinction coefficients, ϵ, of 1 to 100 M^{-1} cm^{-1}) and are responsible for the colors that are generally associated with transition metal complexes. However, at the dilute concentrations available for protein solutions (millimolar or less), most small molecule transition-metal complexes appear to be at most slightly colored. In contrast, many metalloproteins are intensely colored because of absorption bands in the visible spectral region with $\epsilon > 1000$ M^{-1} cm^{-1}. Familiar examples are blue Cu and Fe-S proteins, such as plastocyanin and ferrodoxin. The absorption bands often correspond to ligand-to-metal charge transfer transitions in which an electron is excited from the filled orbitals of the ligand to the partially filled *d* orbitals of the metal. The important point is that the energies and intensities of such transitions sensitively reflect ligand-metal bonding (*4*). For many small molecule transition metal complexes, the charge transfer transitions contribute to the ultraviolet spectral region. However, for strongly colored metalloproteins, intense charge transfer transitions are at a much lower energy and signal the presence of highly covalent ligand-metal bonds, which strongly affect the chemical properties of the metal ion. In this article, we focus on Cu proteins with spectra that are dominated by unique features. The origins of these features are now becoming well understood and provide significant insight into the biological reactivity of these active sites (*2*).

The Cu proteins are generally divided into three classes on the basis of their spectral features (*5*). Small molecule inorganic Cu(II) complexes usually have tetragonal geometries with four strongly coordinated equatorial ligands in the *xy* plane and weaker axial ligands along the *z* axis (Fig. 1A). Antibonding interactions with these ligands split the five *d* orbitals such that the $d_{x^2-y^2}$ level has the highest energy. Because Cu(II) has nine *d* electrons, the ground state has one unpaired electron in the $d_{x^2-y^2}$ orbital (included in Fig. 1A). This ground state gives a characteristic EPR spectrum (Fig. 2A, top) with $g_\parallel > g_\perp > 2.00$ and a large parallel hyperfine splitting $A_\parallel > 140$ G. The hyperfine splitting results from the spin of the unpaired electron coupling to the nuclear spin of the Cu. Differences in the spectra define the three classes of Cu proteins, which exhibit different reactivities.

1) The normal Cu proteins (such as Cu,Zn superoxide dismutase, dopamine β mono-oxygenase, and phenylalanine hydroxylase) exhibit EPR spectra similar to the one in Fig. 2A, top, and absorption spectra in the visible region (Fig. 2B, top) that reveal weak ligand-field transitions that are associated with the Cu center. The electronic structure of normal Cu sites is discussed in (*4*) and is not considered here.

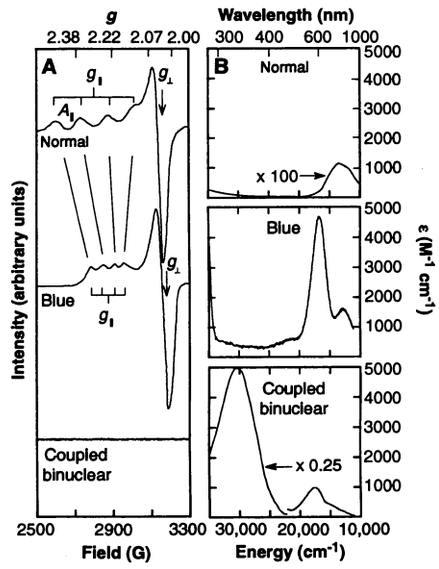

Fig. 2. Comparison of the electron paramagnetic resonance (EPR) (left panel) and electronic absorption spectra (right panels) of normal, blue, and coupled binuclear Cu sites. (**A**) The EPR spectra of $Cu(H_2O)_6^{2+}$ (top), spinach plastocyanin (center), and *Limulus polyphemus* oxyhemocyanin (bottom). (**B**) The corresponding absorption spectra. Note the expanded molar absorptivity scale for $Cu(H_2O)_6^{2+}$ (×100) and the reduced scale (×0.25) for the 350-nm band in oxyhemocyanin.

2) The blue Cu proteins exhibit dramatically different spectral features compared with normal Cu sites. The parallel hyperfine splitting is greatly reduced (Fig. 2A, middle), and there is a strong absorption band ($\epsilon \sim 4700$ M^{-1} cm^{-1}) at ~600 nm (Fig. 2B, middle) that is responsible for the intense blue color of these proteins. The blue Cu proteins include the plastocyanins and azurins and function as electron carriers in electron transport chains. In contrast to normal Cu complexes, the blue Cu proteins generally have high reduction potentials and exhibit high rates of long-range, outer-sphere electron transfer.

3) The coupled binuclear Cu proteins, which include the hemocyanins and tyrosinases, reversibly bind O_2 and, in the case of tyrosinase, activate it for hydroxylation of phenolic substrates. The oxygenated (oxy) form of the coupled binuclear Cu site in hemocyanin involves peroxide bound to two Cu(II) atoms. The absence of an EPR signal (Fig. 2A, bottom) results from the strong antiferromagnetic coupling (spin pairing) between the electrons on each Cu, which is due to the presence of a bridging ligand (*6*). The oxy intermediate of tyrosinase (oxytyrosinase) can be stabilized and has the same spectral features as oxyhemocyanin, which indicates that the active sites are similar (*7*, *8*). The absorption spectrum of the oxy sites of these proteins has two

bands, one at ~600 nm ($\epsilon \sim 1000\ M^{-1}\ cm^{-1}$) and a second, intense band at ~350 nm ($\epsilon \sim 20{,}000\ M^{-1}\ cm^{-1}$) (Fig. 2B, bottom).

The multicopper oxidases, which include laccase, ceruloplasmin, and ascorbate oxidase, couple four one-electron oxidations of substrate to the four-electron reduction of O_2 to H_2O. They contain a combination of all three classes of Cu centers. The simplest multicopper oxidase, laccase, has one center of each class for a total of four Cu ions. For the multicopper oxidases, it is useful to refer to the blue Cu as a type 1 (T1), the normal Cu as a type 2 (T2), and the coupled binuclear Cu as a type 3 (T3) center (*2, 5*). However, the T2 and T3 Cu centers are fundamentally different from those in the single center enzymes in that they form a trinuclear Cu cluster site (*9, 10*) that functions as a unit in the multielectron reduction of O_2 to H_2O.

High-resolution x-ray crystal structures are now available for the blue Cu sites in several proteins (*11*) (Fig. 1B), the coupled binuclear Cu site in oxyhemocyanin from *Limulus polyphemus* (*12*) (Fig. 1C), and the trinuclear Cu cluster site in ascorbate oxidase (*10*) (Fig. 1D). As first predicted by spectroscopy (*13*), the geometry of the blue Cu site is very different from that of normal Cu centers in that it is a distorted tetrahedron with a short cysteine (Cys) thiolate S–Cu bond of 2.13 Å. The remaining three ligands are two imidizole N atoms from histidine (His) residues and a thioether S from methionine (Met) with a very long Cu–S_{Met} bond length of 2.90 Å.

The oxyhemocyanin (and oxytyrosinase) site (Fig. 1C) consists of two tetragonal Cu(II) atoms, each coordinated by two strong equatorial and one weaker axial N_{His} ligand. Spectral studies require that peroxide bridge the two Cu centers (*14*), and Cu model studies by Kitajima *et al.* (*15*) first defined the presence of a side-on (μ-η^2:η^2) peroxide bridging mode in transition metal chemistry. This peroxide bridging mode has recently been determined to be present at the oxyhemocyanin site with the peroxide occupying two equatorial positions on each Cu (*12*) (Fig. 1C).

Low-temperature magnetic circular dichroism (LT-MCD) studies on laccase first defined the presence of a trinuclear (T2 and T3) Cu-cluster site in biology (*9*), which has recently been confirmed by x-ray diffraction studies of ascorbate oxidase (*10*) (Fig. 1D). The two T3 Cu atoms each have three His ligands and are bridged by a hydroxide group. In the crystal structure, these Cu atoms are thought to be tetrahedral. The T2 Cu is described as a three-coordinate center with two His ligands and a hydroxide that is bound opposite to the triangular cluster. All Cu-Cu distances are less than 4.0 Å. Ligand field spectral data indicate that the two T3 Cu atoms are not equivalent and that all three of the Cu atoms in the cluster are better described as having tetragonal geometries (*16*).

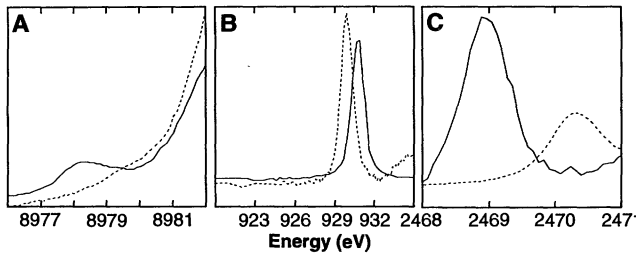

Fig. 3. The x-ray absorption spectroscopy for the blue Cu protein plastocyanin. (**A**) Single crystal, polarized Cu K-edge spectra of plastocyanin with the x-ray beam polarized parallel to the molecular *xy* axes (——) or to the *z* axis (along the thioether S–Cu bond) (----) (*22*). (**B**) The Cu L-edge spectra for the blue Cu protein, plastocyanin (——), and *N*-methylphenethylammonium tetrachlorocuprate (cupric chloride) (----), a normal Cu complex (*23*). (**C**) S K-edge spectra for plastocyanin (——) and tet b, {[*rac*-5,7,7,12,14,14-hexamethyl-1,4,8,11-tetraazocyclotetradecane] Cu(II) *o*-mercaptobenzoate hydrate} (----), a Cu thiolate model complex (*21*).

Proceeding from the geometric structures of these Cu protein active sites, one can correlate spectral data with bonding calculations to develop a detailed description of the electronic structure of these active sites. As summarized below, the distinctive spectral features associated with each of these sites are now understood and reflect electronic structures that make critical contributions to the biological reactivity of the compounds. For the blue Cu site, the small hyperfine splitting and intense low-energy absorption band both result from a highly covalent Cu–S_{Cys} bond that activates this residue for directional, efficient, long-range electron transfer. For oxyhemocyanin and oxytyrosinase, the spectral features reflect an unusual electronic structure for the side-on bridged peroxide that leads to an extremely stable peroxide–Cu bond for reversible O_2 binding in hemocyanin and a greatly weakened O–O bond that activates it for cleavage at the peroxide level in the mono-oxygenase chemistry of tyrosinase. For the trinuclear Cu cluster site, new spectral data demonstrate that it has a fundamentally different interaction with O_2 relative to hemocyanin and tyrosinase (*17*), which generates a peroxide intermediate (*18*) that has a different geometric and electronic structure from the side-on bridged structure. This difference directly correlates with differences in biological function; O_2 binding and activation for hemocyanin and tyrosinase versus irreversible reduction of O_2 to H_2O at the trinuclear Cu cluster site in the multicopper oxidases.

Blue Copper Sites: Electron Transfer

The blue Cu site has an EPR spectrum with $g_{\|} > g_{\perp} > 2.00$ (Fig. 2A), which means that the ground state involves a half-occupied Cu $d_{x^2-y^2}$ orbital. This orbital takes up and transfers an electron in the biological reactivity of this active site. Single crystal EPR studies on plastocyanin have determined that the $g_{\|}$ direction is almost parallel to the Cu–S_{Met} bond (Fig. 1B) (*19*), which defines the *z* axis of the site and places the $d_{x^2-y^2}$ orbital perpendicular to this direction, within 15° of the plane defined by the two N_{His} and S_{Cys} ligands.

It had generally been thought that the small hyperfine splitting in the EPR spectrum of the blue Cu site (Fig. 2A) originated from Cu $4p_z$ mixing into this $d_{x^2-y^2}$ orbital (*20*) (an electron in a p_z orbital has a hyperfine interaction with the nucleus of the Cu atom that is opposite that of an electron in a $d_{x^2-y^2}$ orbital). This was tested experimentally with polarized single-crystal x-ray absorption spectroscopy at the Cu K-edge (*21*). The x-ray absorption peak at 8979 eV (Fig. 3A) corresponds to the Cu 1*s* $\rightarrow \sqrt{1-\alpha^2}\,Cu\ d_{x^2-y^2} + \alpha Cu\ 4p$ transition. As only the 1*s* $\rightarrow$ 4*p* component is electric-dipole allowed, the intensity at 8979 eV probes the nature of Cu 4*p* mixing. Polarized x-ray absorption spectra were taken with the electric vector of light either parallel to the molecular *z* or to the *xy* axes (*22*). From the data shown in Fig. 3A, the 8979-eV peak is *xy* polarized, which implies that all Cu 4*p* mixing involves the $4p_{x,y}$ orbitals and $4p_z$ mixing is not the mechanism that reduces hyperfine coupling in the blue Cu sites. This result allowed us to focus on the alternative mechanism for the reduction of the hyperfine interaction, which is a highly covalent active site. The idea is that delocalization of the unpaired electron onto the ligands reduces its coupling to the nuclear spin of the Cu.

We experimentally probed the extent of covalency in the blue Cu site through Cu L-edge absorption studies (*23*). The blue Cu site exhibits an absorption peak at 930 eV (Fig. 3B) that corresponds to an electric-dipole–allowed Cu 2*p* $\rightarrow$ Cu $3d_{x^2-y^2}$ transition. Its intensity quantitates the amount of Cu 3*d* character in the ground-state wave function. Its intensity is 0.61 times that of the 2*p* $\rightarrow$ $3d_{x^2-y^2}$ transition in tetragonal cupric chloride, which is well

defined to have 61% Cu *d* character in its ground-state wave function. Thus, the blue Cu site is very covalent with only ~38% Cu $d_{x^2-y^2}$ character in the half-occupied molecular orbital.

Self-consistent-field Xα scattered-wave (SCF-Xα-SW) bonding calculations first indicated that this site is strongly delocalized onto the S_{Cys} ligand (*24, 25*) (see below). This result was experimentally confirmed through S K-edge x-ray absorption spectral studies (*21*). The blue Cu site exhibits an intense band at 2469 eV (Fig. 3C), which corresponds to the S 1*s* → $\sqrt{1-\beta^2}$ Cu $3d_{x^2-y^2} - \beta S_{Cys}3p$ transition. The 1*s* orbital is localized on the S atom, so the intensity of the 2469-eV band reflects the amount of S 3*p* character in the half-occupied orbital. The intensity of this peak in plastocyanin is 2.55 times that of a well-defined Cu thiolate model complex, tet b (*26*) (Fig. 3C), which has ~15% S covalent character. Thus, the blue Cu site has ~38% S_{Cys} character in the highest energy half-occupied molecular orbital.

A final key feature of the ground-state wave function came from the detailed assignment of the characteristic optical absorption spectrum of the blue Cu site (Fig. 2B, middle), which was obtained from a combination of polarized single crystal absorption and LT-MCD spectroscopies (*25*). The intense absorption band at 600 nm corresponds to the $S_{Cys}\pi \rightarrow$ Cu $d_{x^2-y^2}$ charge transfer transition, and the $S_{Cys}\sigma \rightarrow$ Cu $d_{x^2-y^2}$ charge transfer transition is a weak band to higher energy. Normally, σ charge transfer transitions are intense, and π charge transfer is weak. Because the intensity of a charge transfer reflects the overlap of the donor and acceptor orbitals involved in the transition, the $d_{x^2-y^2}$ orbital must be rotated in the *xy* plane such that its lobes are bisected by the Cu–S_{Cys} bond, rather than lying along the bond, as in normal Cu complexes.

The above experimental description of the ground state of the blue Cu site is in excellent agreement with the results of SCF-Xα-SW calculations (*24, 25*). We superimposed the ground-state wave function onto the Cu site in plastocyanin (*27*) (Fig. 4). This ground state involves a $d_{x^2-y^2}$ orbital that is in the plane defined by the two N_{His} and S_{Cys} ligands and has its lobes bisected by the Cu–S_{Cys} bond. This orbital is highly covalent, and the delocalization is strongly anisotropic, involving the *p*π orbital of the thiolate S. As shown in Fig. 4 (inset), the blue Cu site in plastocyanin is buried in the protein (*11*). There are two surface patches that are believed to be involved in electron transfer.

The adjacent patch is ~6.5 Å from the Cu, through the His^{87} ligand, and the remote patch is ~12.5 Å from the Cu but is connected through a protein pathway that involves the Cys^{84} ligand, which is covalently linked to tyrosine (Tyr) 83 (*28*). A similar 12.5 Å pathway (with His replacing Tyr) is present in the blue copper–containing enzymes ascorbate oxidase (*10*) and nitrite reductase (*29*). On the basis of distance considerations alone, the adjacent patch is expected to be orders of magnitude more efficient at electron transfer (*30*); however, both surface patches have comparable electron transfer rates (*28*). Importantly, the ground-state wave function, shown in Fig. 4, is extremely well suited for rapid, long-range electron transfer to the remote patch. The electron transfer matrix element, which describes the electronic contribution to the electron transfer rate, is proportional to the square of the ligand character in the ground-state wave function (*30*). The high anisotropic covalency of the wave function thus strongly activates the Cys ligand for electron transfer to the remote patch. The existence of a low-energy, intense $S_{Cys}\pi \rightarrow$ Cu $d_{x^2-y^2}$ charge transfer absorption band thus reflects the presence of an efficient hole superexchange mechanism for rapid, directional, long-range electron transfer in the blue Cu proteins.

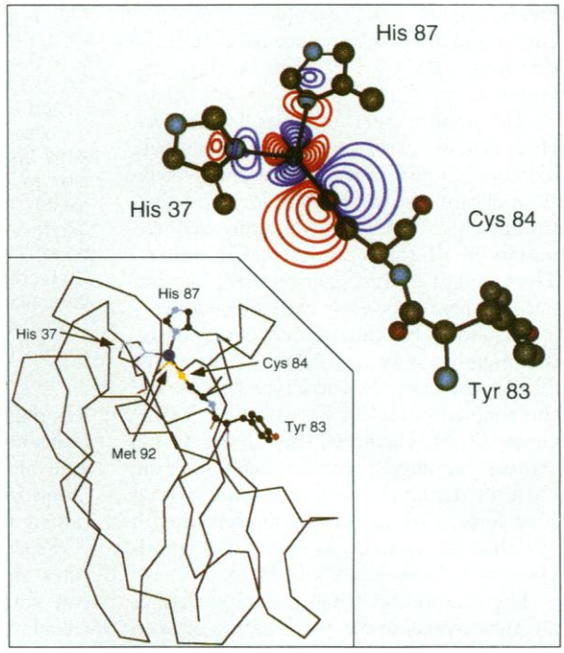

Fig. 4. Proposed electron transfer pathway in plastocyanin. The inset shows a Cα plot with the side groups of the Cu-coordinating ligands His^{37}, His^{87}, Cys^{84}, and Met^{92}, as well as the remote path Tyr^{83} (*11, 48*). The remote electron transfer pathway (Cu-Cys^{84}-Tyr^{83}) is shown in a view down the Cu–S_{Met} bond (the Met group has been removed for clarity). The wave function obtained from the self-consistent-field Xα scattered wave (SCF-Xα-SW) calculations has been superimposed onto the crystallographic coordinates to show the highly covalent Cu–S_{Cys} bond (*27*). Wave function contour levels are displayed at ±0.32, ±0.16, ±0.08, ±0.04, ±0.02, and ±0.01 $(e/bohr^3)^{1/2}$.

Coupled Binuclear Copper Sites: O_2 Binding and Activation

The side-on bridging structure of the peroxide that is bound to the binuclear cupric site in oxyhemocyanin (and oxytyrosinase) (Fig. 1C) is quite unusual and results in an electronic structure (*31*) that is different than that of the generally occurring end-on bridging structure (*32*). The electronic structures for both geometries (Fig. 5) are reflected in the energy splitting of the highest occupied molecular orbital (HOMO) and lowest unoccupied molecular orbital (LUMO) (that is, the symmetric and antisymmetric combinations of the $d_{x^2-y^2}$ orbitals on each Cu) that is caused by bonding interactions with the peroxide. For the end-on geometry, the dominant interaction involves the highest energy occupied π antibonding orbital (π^*_σ) on the peroxide, which is stabilized by a σ bonding interaction with both Cu atoms that raises the energy of the LUMO. This results in the donation of electron density from this peroxide π^*_σ orbital onto the Cu atoms.

In the side-on bridging structure, the peroxide π^*_σ orbital again acts as a σ donor to the Cu atoms. The bonding-antibonding interaction in this geometry, however, is much larger than in the end-on structure. The origin of this increased σ donor bonding of the peroxide can be seen in the contour diagrams for both LUMOs (Fig. 5). The peroxide π^*_σ orbital has two σ bonding interactions with each Cu in the side-on structure, as opposed to one σ interaction per Cu in the end-on geometry. The side-on bridging structure has an additional bonding interaction that had not been previously observed for peroxide. As can be seen in the energy level diagram (Fig. 5), the HOMO is stabilized by a bonding interaction with the high-energy unoccupied σ antibonding orbital on the peroxide. The HOMO contour shows that this bonding interaction shifts some electron density from the Cu atoms onto the peroxide. Thus, in the side-on bridging structure, peroxide also functions as a π acceptor

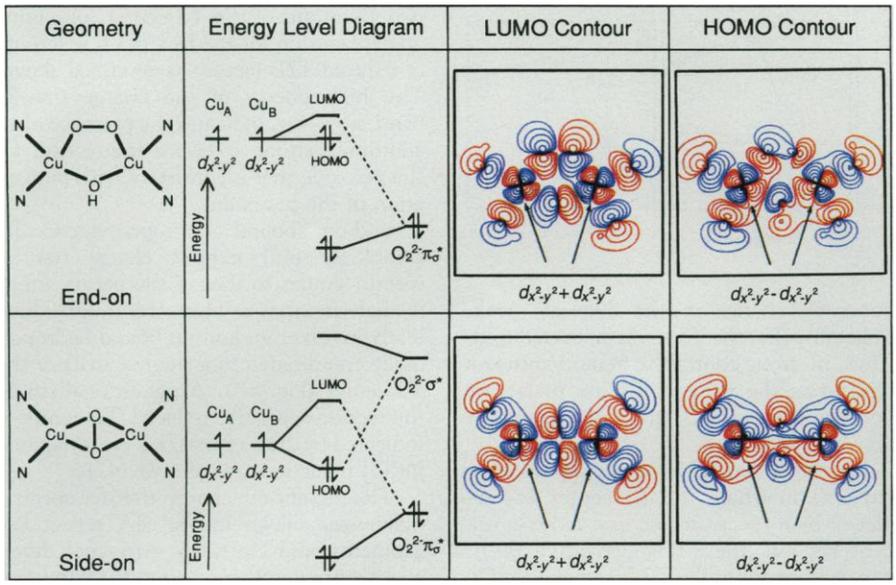

Fig. 5. Electronic structures of end-on (*cis*-μ-1,2) and side-on (μ-η^2:η^2) peroxide bridged binuclear cupric model complexes. The HOMO and LUMO wave function contours are obtained from broken-symmetry SCF-Xα-SW calculations (*31*). The labels Cu_A and Cu_B refer to the two Cu atoms in the dimer.

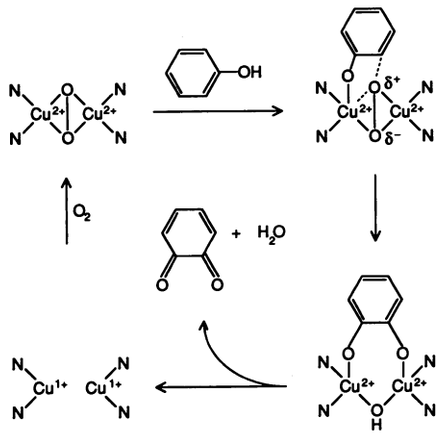

Fig. 6. Proposed mechanism for oxytyrosinase applied to the side-on bridged peroxide structure. The axial N_{His} ligands on each Cu have been removed for clarity.

ligand using its σ* orbital, which is strongly antibonding with respect to the O–O bond.

The spectral features of the oxyhemocyanin and oxytyrosinase active sites directly reflect this unusual electronic structure for the side-on bridging peroxide (Fig. 5). First, the lack of an EPR signal (Fig. 2A, bottom) results from strong antiferromagnetic coupling between the two Cu atoms. This coupling is proportional to the HOMO-LUMO splitting that is caused by bonding interactions with the bridging ligand (*33*). For the side-on bridging structure, this splitting is extremely large because of the combination of the very strong σ donor bonding (which raises the energy of the LUMO) and π acceptor bonding (which lowers the energy of the HOMO) with the peroxide.

Second, the 350-nm absorption band (Fig. 2B, bottom) corresponds to the transition of an electron from the π^*_σ orbital on the peroxide to the half-occupied $d_{x^2-y^2}$ orbitals on the two Cu atoms (*14*). This transition is far more intense and at much higher energy than peroxide $\pi^*_\sigma \rightarrow$ Cu charge transfer transitions (*34*) in end-on bound peroxide Cu complexes (*35*). Both the high energy of this band and its strong intensity (which is proportional to the square of orbital overlap) are a result of the very strong σ donor interaction of the peroxide with the binuclear cupric site, which is caused by the two bonding interactions with each Cu in the side-on structure.

The third spectral feature, which is in the resonance Raman spectrum is a very low energy O–O stretching vibration at 750 cm^{-1} (*36*). Complexes of Cu and end-on bound peroxide, prepared by Karlin *et al.* (*35*), exhibit ν_{o-o} stretching frequencies in the range of 800 to 850 cm^{-1} (*34*). The very strong σ donor interaction of the side-on structure should increase the O–O bond strength, and hence increase ν_{o-o}, as this removes electron density from the π antibonding orbital on the peroxide. In fact, the reduced energy of the O–O vibration in oxyhemocyanin and oxytyrosinase reflects an extremely weak O–O bond in the side-on structure. This results from the presence of the π acceptor interaction, which shifts electron density into the highly antibonding peroxide σ* orbital.

The unusual electronic structure of the side-on bridging geometric structure would appear to make significant contributions to biological function. The combination of strong σ donor and π acceptor bonding leads to a very stable peroxide-Cu bond in oxyhemocyanin and is particularly important with respect to limiting the loss of peroxide from the oxy site, which would result in a binuclear cupric site which would be inactive in reversible O_2 binding. The electronic structure (Fig. 5) should also produce a highly activated peroxide molecule in oxytyrosinase. The strong σ donor interaction results in a less negative peroxide, whereas the π acceptor interaction into the peroxide σ* orbital greatly weakens the O–O bond, activating it for cleavage. As illustrated in Fig. 6, tyrosinase has a highly accessible active site (*8*) (relative to hemocyanin) where the phenolic substrate coordinates directly to the Cu (*37*). This would lead to donation of electron density from the substrate into the LUMO, which is antibonding with respect to both the O–O and Cu–O bonds and should initiate oxygen transfer to the *ortho* position on the phenyl ring. The resultant coordinated catecholate will transfer two electrons to the binuclear cupric site, leading to the dissociative elimination of the *o*-quinone product and the formation of the deoxy site for further turnover.

Trinuclear Copper-Cluster Sites: O_2 Reduction to H_2O

Spectroscopic studies on a multicopper oxidase, laccase (which contains one T1 center and one each of T2 and T3 centers that form a trinuclear Cu cluster, as pictured for ascorbate oxidase in Fig. 1D), demonstrate that the trinuclear Cu cluster site exists (*9*) and has a fundamentally different geometric and electronic structure relative to the coupled binuclear Cu site in hemocyanin and tyrosinase (*17, 38*). The difference is caused by the strong influence of the T2 Cu on the T3 center and directly correlates with the difference in biological function: laccase catalyzes the four-electron reduction of O_2 to H_2O. Originally, the T3 site was thought to be similar to the coupled binuclear Cu site in hemocyanin (and tyrosinase) with a similar O_2 reactivity (*39*). As seen from the structures (Fig. 1C and T3 in Fig. 1D), both sites have three His residues on each Cu atom. In addition, the displacement of peroxide from oxyhemocyanin results in a binuclear cupric site that is strongly antiferromagnetically coupled (*40*), indicating that a hydroxide bridge (*41*) has replaced the peroxide in Fig. 1C, which results in a structure similar to that of the T3 center in Fig. 1D. However, there is a striking differ-

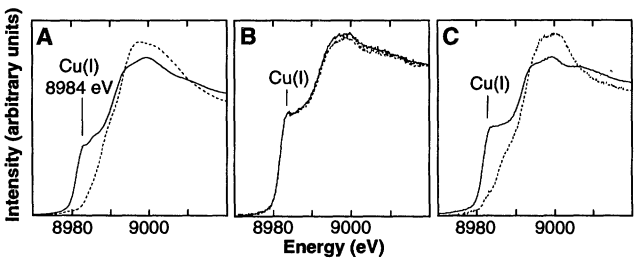

Fig. 7. The O_2 reactivity of deoxyhemocyanin and reduced laccase derivatives. The Cu K x-ray absorption edges for (**A**) deoxyhemocyanin, (**B**) reduced T2D laccase, and (**C**) reduced T1Hg laccase before (——) and after (----) reaction with O_2.

ence in the O_2 reactivity of deoxyhemocyanin and deoxytyrosinase relative to that of the reduced T3 site in laccase.

Deoxyhemocyanin contains a binuclear cuprous site that reversibly binds O_2, producing the oxy site in Fig. 1C. The x-ray absorption spectrum of deoxyhemocyanin exhibits a peak at 8984 eV, which is characteristic of reduced Cu, that is eliminated upon O_2 binding, indicating that the site is oxidized to the binuclear cupric level in oxyhemocyanin (*42*) (Fig. 7A).

A derivative of laccase can be prepared (*43*) in which the T2 Cu is reversibly removed (the type 2 depleted, or T2D, derivative), which leaves an isolated T3 center [it should be noted from the crystal structure of ascorbate oxidase (*10*) that the T1 Cu is at a distance of ~12.5 Å from the T3 center]. As shown in Fig. 7B, reaction of a fully reduced T3 center with O_2 produces no change in the 8984-eV peak, indicating that the T3 site remains reduced. Thus, in strong contrast to hemocyanin and tyrosinase, the reduced T3 site in laccase does not react with O_2 in the absence of the T2 Cu (*17*).

A second derivative of laccase was studied (*17*) in which the T1 center was replaced by a spectroscopic and redox-innocent Hg ion [the T1Hg derivative (*44*)], which leaves only the T2-T3 trinuclear Cu cluster. Reduction of the T1Hg derivative again leads to a large Cu(I) peak at 8984 eV (Fig. 7C); however, reaction of the fully reduced trinuclear Cu cluster site with O_2 rapidly eliminates this peak, which means that the Cu atoms have been oxidized. Thus, the trinuclear Cu cluster site is the minimum structural unit required for O_2 reduction.

The presence of the Hg^{2+} ion in the T1 center results in one less electron that is available for reduction of O_2, enabling us to stabilize an oxygen intermediate of T1Hg laccase (*18*). Studies of x-ray absorption and MCD spectra of this intermediate have shown that the two T3 Cu atoms are oxidized and the T2 center is reduced. Thus, two electrons have been transferred to O_2, which results in a peroxide level intermediate at the trinuclear Cu cluster site. This intermediate is produced at a rate that is consistent with the reduction of O_2 by native laccase.

The charge transfer absorption spectrum of this peroxy intermediate of laccase was compared to the peroxide-to-Cu(II) charge transfer spectrum of oxyhemocyanin and oxytyrosinase (Fig. 8A). These spectra clearly show major differences that indicate a significant change in the geometric and electronic structure for the peroxide-Cu bond in laccase relative to that of oxyhemocyanin and oxytyrosinase (Fig. 1C). Although detailed spectral studies on this intermediate are still needed (*45*), preliminary structural insight is available from the charge transfer data. The charge transfer intensity of the peroxy intermediate is less than one-quarter as strong as that of oxyhemocyanin and oxytyrosinase, which indicates that the peroxide is likely bound to only one Cu(II) of the oxidized T3 site. Thus, in contrast to oxyhemocyanin and oxytyrosinase, peroxide does not bridge the two Cu atoms of the T3 center, providing an explanation for the lack of O_2 reactivity of reduced T2D laccase as described above. The high energy of the charge transfer band, however, indicates the presence of an additional strong σ donor interaction for the peroxide that is consistent with protonation of the peroxide.

End-on bound hydroperoxide-Cu(II) complexes (*46*) exhibit charge transfer spectra similar to that of the peroxy intermediate in laccase. Thus, this intermediate likely involves an end-on bound hydroperoxide coordinated to a single Cu(II) of the T3 center (Fig. 8B). An additional strong interaction with the reduced T2 center is indicated by the fact that this Cu is required for O_2 reduction (see above) (*47*).

The significant charge transfer spectral differences shown in Fig. 8A reflect key geometric and electronic structural differences for peroxide binding to the trinuclear Cu cluster site in laccase as compared with hemocyanin and tyrosinase (Fig. 8B), which should relate to their differences in biological function. The side-on bridging of oxyhemocyanin and oxytyrosinase should stabilize the bound peroxide and activate its O–O bond cleavage for hydroxylation, whereas the end-on binding of hydroperoxide appears to promote its irreversible further reduction to H_2O at the trinuclear Cu cluster site. Further research is needed to define key electronic structural differences associated with this geometric difference and to evaluate their contribution to the oxidase reactivity of the trinuclear Cu cluster site.

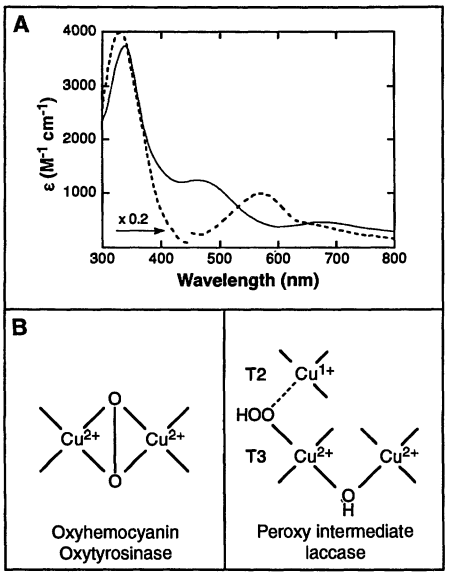

Fig. 8. Comparison of peroxide binding in oxyhemocyanin and oxytyrosinase with the oxygen intermediate in laccase. (**A**) Absorption spectra of the peroxide level intermediate of T1Hg laccase (——) and oxyhemocyanin and oxytyrosinase (----). The higher energy region of the oxyhemocyanin-oxytyrosinase spectrum is scaled down fivefold. (**B**) Active site structure of oxyhemocyanin and oxytyrosinase (coupled binuclear) and the proposed structure of the peroxide level intermediate of laccase (trinuclear Cu cluster).

Concluding Comments

It should be clear from the above discussion that the distinctive spectral features associated with many classes of metalloprotein active sites in bioinorganic chemistry indicate the presence of unusual electronic structures. These certainly reflect geometric structure; however, importantly, the electronic structures can make significant contributions to the reactivity of active sites in catalysis. This is an exciting frontier in the field of bioinorganic chemistry and is relevant to many other fields of chemistry, including surface science and heterogeneous catalysis.

REFERENCES AND NOTES

1. J. Kim and D. C. Rees, *Science* **257**, 1677 (1992).
2. E. I. Solomon, M. J. Baldwin, M. D. Lowery, *Chem. Rev.* **92**, 521 (1992).
3. E. I. Solomon and Y. Zhang, *Acc. Chem. Res.* **25**, 343 (1992).
4. E. I. Solomon, *Comments Mod. Chem. A* **3**, 225 (1984); ——, M. D. Lowery, L. B. LaCroix, D. E. Root, *Methods Enzymol.*, in press.
5. E. I. Solomon, K. W. Penfield, D. E. Wilcox, *Struct. Bonding* **53**, 1 (1983); T. G. Spiro, Ed., *Metal Ions in Biology* (Wiley, New York, 1981), vol. 3; J. A.

Fee, *Struct. Bonding* **23**, 1 (1975); R. Malkin and B. G. Malmström, *Adv. Enzymol. Relat. Subj.* **33**, 177 (1970).
6. E. I. Solomon *et al.*, *J. Am. Chem. Soc.* **98**, 1029 (1976); D. M. Dooley, R. A. Scott, J. Ellinghaus, E. I. Solomon, H. B. Gray, *Proc. Natl. Acad. Sci. U.S.A.* **75**, 3019 (1978).
7. R. L. Jolley, Jr., L. H. Evans, N. Makino, H. S. Mason, *J. Biol. Chem.* **249**, 335 (1974).
8. R. S. Himmelwright, N. C. Eickman, C. D. LuBien, K. Lerch, E. I. Solomon, *J. Am. Chem. Soc.* **102**, 7339 (1980); N. C. Eickman *et al.*, *ibid.* **100**, 6529 (1978).
9. M. D. Allendorf, D. J. Spira, E. I. Solomon, *Proc. Natl. Acad. Sci. U.S.A.* **82**, 3063 (1985); D. J. Spira-Solomon, M. D. Allendorf, E. I. Solomon, *J. Am. Chem. Soc.* **108**, 5318 (1986).
10. A. Messerschmidt *et al.*, *J. Mol. Biol.* **224**, 179 (1992).
11. P. M. Coleman *et al.*, *Nature* **272**, 319 (1978); J. M. Guss and H. C. Freeman, *J. Mol. Biol.* **169**, 521 (1983); E. T. Adman, *Adv. Protein Chem.* **42**, 145 (1991).
12. K. Magnus and H. Ton-That, *J. Inorg. Biochem.* **47**, 20 (1992); K. Magnus *et al.*, personal communication.
13. E. I. Solomon, J. W. Hare, H. B. Gray, *Proc. Natl. Acad. Sci. U.S.A.* **73**, 1389 (1976).
14. N. C. Eickman, R. S. Himmelwright, E. I. Solomon, *ibid.* **76**, 2094 (1979).
15. N. Kitajima, K. Fujisawa, Y. Moro-oka, *J. Am. Chem. Soc.* **111**, 8975 (1989).
16. J. L. Cole, P. A. Clark, E. I. Solomon, *ibid.* **112**, 9534 (1990).
17. J. L. Cole, G. O. Tan, E. K. Yang, K. O. Hodgson, E. I. Solomon, *ibid.*, p. 2243.
18. J. L. Cole, D. P. Ballou, E. I. Solomon, *ibid.* **113**, 8544 (1991).
19. K. W. Penfield *et al.*, *ibid.* **103**, 4382 (1981).
20. C. A. Bates, W. S. Moore, K. J. Standley, K. W. H. Stevens, *Proc. Phys. Soc.* **79**, 73 (1962); A. S. Brill and G. F. Bryce, *J. Chem. Phys.* **48**, 4398 (1968); J. E. Roberts, T. G. Brown, B. M. Hoffman, J. Peisach, *J. Am. Chem. Soc.* **102**, 825 (1980).
21. S. E. Shadle *et al.*, *J. Am. Chem. Soc.* **115**, 767 (1993).
22. R. A. Scott, J. E. Hahn, S. Doniach, H. C. Freeman, K. O. Hodgson, *ibid.* **104**, 5364 (1982).
23. S. J. George, M. D. Lowery, E. I. Solomon, S. P. Cramer, *ibid.*, in press.
24. K. W. Penfield, A. A. Gewirth, E. I. Solomon, *ibid.* **107**, 4519 (1985).
25. A. A. Gewirth and E. I. Solomon, *ibid.* **110**, 3811 (1988).
26. J. L. Hughey IV *et al.*, *ibid.* **101**, 2617 (1979).
27. M. D. Lowery, J. A. Guckert, M. S. Gebhard, E. I. Solomon, *ibid.*, in press.
28. A. G. Sykes, *Struct. Bonding* **75**, 175 (1991); *Adv. Inorg. Chem.* **36**, 377 (1991).
29. J. W. Godden *et al.*, *Science* **253**, 438 (1991).
30. G. A. Palmer, Ed., *Struct. Bonding* **75**, 1–233 (1991); R. A. Marcus and N. Sutin, *Biochim. Biophys. Acta* **811**, 265 (1985); M. D. Newton, *Chem. Rev.* **91**, 767 (1991).
31. P. K. Ross and E. I. Solomon, *J. Am. Chem. Soc.* **113**, 3246 (1991); M. J. Baldwin *et al.*, *ibid.* **114**, 10421 (1992).
32. E. C. Niederhoffer, J. H. Timmons, A. E. Martell, *Chem. Rev.* **84**, 137 (1984).
33. P. J. Hay, J. C. Thibeault, R. Hoffman, *J. Am. Chem. Soc.* **97**, 4884 (1975).
34. J. E. Pate, R. W. Cruse, K. D. Karlin, E. I. Solomon, *ibid.* **109**, 2624 (1987); M. J. Baldwin *et al.*, *ibid.* **113**, 8671 (1991).
35. R. R. Jacobson *et al.*, *ibid.* **110**, 3690 (1988); K. D. Karlin *et al.*, *ibid.* **109**, 2668 (1987).
36. T. B. Freedman, J. S. Loehr, T. M. Loehr, *ibid.* **98**, 2809 (1976); J. A. Larrabee *et al.*, *ibid.* **99**, 1979 (1977); J. A. Larrabee and T. G. Spiro, *ibid.* **102**, 4217 (1980).
37. M. E. Winkler, K. Lerch, E. I. Solomon, *ibid.* **103**, 7001 (1981); D. E. Wilcox *et al.*, *ibid.* **107**, 4015 (1985).
38. D. J. Spira-Solomon and E. I. Solomon, *ibid.* **109**, 6421 (1987).
39. O. Farver, M. Goldberg, I. Pecht, *FEBS Lett.* **94**, 383 (1978); B. Reinhammar, *J. Inorg. Biochem.* **15**, 27 (1981); in *Copper Proteins and Copper Enzymes*, R. Lontie, Ed. (CRC Press, Boca Raton, FL, 1984), vol. 3, pp. 1–36.
40. D. E. Wilcox, J. R. Long, E. I. Solomon, *J. Am. Chem. Soc.* **106**, 2186 (1984).
41. A. Volbeda and W. G. J. Hol, *J. Mol. Biol.* **209**, 249 (1989).
42. G. L. Woolery, L. Powers, M. Winkler, E. I. Solomon, T. G. Spiro, *J. Am. Chem. Soc.* **106**, 86 (1984); J. M. Brown, L. Powers, B. Kincaid, J. A. Larrabee, T. G. Spiro, *ibid.* **102**, 4210 (1980); M. S. Co, K. O. Hodgson, T. K. Eccles, R. Lontie, *ibid.* **103**, 984 (1981); K. H. Nakagawa, D. E. Root, K. O. Hodgson, E. I. Solomon, unpublished results.
43. M. T. Graziani, L. Morpurgo, G. Rotilio, B. Mondovì, *FEBS Lett.* **70**, 87 (1976).
44. M. M. Morie-Bebel, M. C. Morris, J. L. Menzie, D. R. McMillin, *J. Am. Chem. Soc.* **106**, 3677 (1984).
45. J. L. Cole, G. O. Tan, B. L. Hemming, K. O. Hodgson, E. I. Solomon, unpublished results.
46. K. D. Karlin *et al.*, *J. Am. Chem. Soc.* **110**, 6769 (1988).
47. Preliminary crystallographic results for peroxide added to fully oxidized ascorbate oxidase seem to also indicate a hydroperoxide bound end on to one T3 Cu. There are, however, differences with respect to bridging ligation relative to the model in Fig. 8B. These differences may relate to the fact that the x-ray data are for a peroxide adduct of the resting enzyme rather than the oxygen intermediate. A. Messerschmidt, in *Bioinorganic Chemistry of Copper*, K. D. Karlin and Z. Tyeklár, Eds. (Chapman & Hall, New York, in press).
48. Plastocyanin coordinates obtained from the Brookhaven Protein Data Bank file 1PCY; F. C. Bernstein *et al.*, *J. Mol. Biol.* **112**, 535 (1977).
49. This research has been supported by the NSF CHE-9217628 for the blue Cu studies) and the NIH (DK-31450 for the coupled binuclear and multicopper studies). E.I.S. expresses his appreciation to all his students and collaborators who are listed as co-authors in the cited literature for their commitment and contributions to this science.

Coherent Control of Quantum Dynamics: The Dream Is Alive

Warren S. Warren, Herschel Rabitz, Mohammed Dahleh

Current experimental and theoretical progress toward the goal of controlling quantum dynamics is summarized. Two key developments have now revitalized the field. First, appropriate ultrafast laser pulse shaping capabilities have only recently become practical. Second, the introduction of engineering control concepts has put the required theoretical framework on a rigorous foundation. Extrapolations to determine what is realistically possible are presented.

Since the early days of quantum mechanics, an implicit dream has been the desire to manipulate and control quantum-mechanical phenomena. This dream crystallized into an active pursuit with the development of the first high-power pulsed lasers in the 1960s. The objectives were focused toward manipulating events at the molecular scale. Special emphasis was given to the goal of selectively breaking bonds in polyatomic molecules, as this capability could, in principle, significantly improve chemists' ability to build and otherwise alter complex molecular frameworks with high specificity. With this objective in mind, a flurry of activity ensued, extending over some 30 years, by chemists and physicists attempting especially to selectively break one bond versus another in polyatomic molecules, using a variety of laser sources (*1*). The basic approach seemed simple: identify the local mode frequency associated with the targeted bond, then pump intensely with a laser tuned to that frequency until the bond breaks.

Many years of work and variations on this theme were attempted, with essentially no substantial success. The crux of the problem eventually became clear: in all but the smallest molecules, locally deposited energy very rapidly redistributes throughout the molecule, destroying the selectivity. As a result, while these studies revealed a great deal about intramolecular energy redistribution, they made the dream lose much of its allure.

In fact, this early paradigm effectively ignored a key aspect of quantum phenomena—quantum dynamical processes are wave phenomena, subject to constructive and destructive interferences. In the past few years, a resurgence of activity has occurred in this field as researchers have finally recognized that actively manipulating these constructive and destructive interferences is the essential step. This recognition has both theoretical and experimental components. On the theoretical side, the active manipulation of quantum dynamics phenomena is now realized to be a problem of control theory or optimal design analogous to efforts carried out in the traditional macroworld engineering disciplines, where the control of airplanes or mechanical and electrical devices is commonplace. The introduction of control theory concepts has finally put the subject of active manipula-

W. S. Warren and H. Rabitz are in the Department of Chemistry, Princeton University, Princeton, NJ 08544, and the Princeton Center for Photonics and Opto-Electronic Materials. M. Dahleh is in the Department of Mechanical Engineering, University of California, Santa Barbara, CA 93106.